Available online at www.sciencedirect.com
SCIENCE DIRECT®
ELSEVIER
International Journal of Solids and Structures 43 (2006) 4201–4219
INTERNATIONAL JOURNAL OF SOLIDS and STRUCTURES
www.elsevier.com/locate/ijsolstr

Shakedown analyses for rolling and sliding contact problems

Alan R.S. Ponter [a], H.F. Chen [a,*], M. Ciavarella [b], G. Specchia [c]

[a] *Department of Engineering, University of Leicester, Leicester LE1 7RH, UK*
[b] *CEMEC-PoliBA – Centre of Excellence in Computational Mechanics, V. le Japigia 182, Politecnico di Bari, 70125 Bari, Italy*
[c] *Politecnic di Bari, Italy*

Received 31 May 2005
Available online 22 July 2005

Abstract

There is a range of problems where repeated rolling and sliding contact occurs over a half space of an elastic–perfectly plastic material. For such problems shakedown and limit analysis provide significant advantages over other forms of analysis when a global understanding of deformation behaviour is required. In this paper, a recently developed numerical upper bound method, the Linear Matching Method (LMM), for shakedown analyses is applied to the solution of a problem previously considered by Ponter et al. [Ponter, A.R.S., Hearle, A.D., Johnson, K.L., 1985. J. Mech. Phys. Solids 33 (4), 339–362] for a moving Hertzian contact, with sliding friction. This semi-analytic solution is an upper bound based on certain specific kinematic assumptions. We show that the Ponter, Hearle and Johnson solution is a reasonable approximate solution for a circular contact area but is less accurate for an elliptic contact area. For an elliptic contact area LLM solutions converge to the line contact solution. The effect of the non-coincidence of the direction of travel and slide is also investigated.

Keywords: Plasticity; Limit loads; Shakedown; Hertzian contact

1. Introduction

The problem of the deformation of surfaces subjected to repeated rolling and sliding contact is a significant problem in number of areas of engineering design. For metallic surfaces rolling contact occurs in bearings and in the contact region of railway wheels and lines. The failure of such surfaces is often associated with the accumulation of strain near the surface. A particularly effective way of gaining insight into the combination of loads at which such strain growth initiates is to evaluate the loads corresponding to the

* Corresponding author.
E-mail addresses: asp@le.ac.uk (A.R.S. Ponter), hfc3@le.ac.uk (H.F. Chen).

0020-7683/$ - see front matter © 2005 Elsevier Ltd. All rights reserved.
doi:10.1016/j.ijsolstr.2005.05.046

shakedown limit for the problem, using the upper and lower bound shakedown theorems for an elastic–perfectly plastic material.

Ponter et al. (1985) discussed the application of the upper bound shakedown theorem to such problems and showed that, for a von Mises yield condition, mechanism of deformation consisted of slip surfaces that surrounded the contact area and allowed a region of the surface to slide forward in the direction of travel of the rolling contact. Such mechanisms are capable of providing the exact solution under the assumption that the associated displacements, in the exact solution, were only in the direction of travel, i.e. there was no "ploughing" component to the deformation field. With this insight, it is then possible to evaluate a minimum upper bounds corresponding to a particular slip surface. The problem discussed by Ponter et al. (1985) is shown as Fig. 1 where a Hertzian contact pressure due to a normal load P is applied to a circular or elliptical region on a half space, together with a friction tangential force fP due to sliding in the direction of travel where f is a coefficient of friction. The contacting loads repeatedly travel along a straight line in the x direction. For a circular contact region their solution forms an interaction diagram, shown in Fig. 2, with axis given by P, in non-dimensional form, and f. Note that k denotes the yield stress under pure shear. The diagram is subdivided into a number of regions. In the Elastic region, purely elastic behaviour occurs and there is no plastic deformation, assuming the body was initially stress free. In the Elastic Shakedown region, there will be some plastic strains during the first few traverses but subsequently the behaviour is purely elastic. In the Plastic Shakedown region, local reverse cycles of plastic strains occur beneath the surface but there is no overall cyclic growth of strain. In the Ratcheting region, cyclic growth of strain occurs. This interaction diagram, Fig. 2, has been widely used since its publication as the basis for design. Recent examples of authors who have used this solution include Ekberg et al. (2002), Ringsberg (2001) and Ringsberg and Josefson (2001).

There is, however, an inherent weakness in the approach, the need to make specific assumptions about the particular classes of deformation modes that occur at shakedown. Ponter et al. (1985) note that their solution fails to converge to the line contact solution for an elliptic contact region for $b/a = 10$, where b and a are the ellipse axes perpendicular to and in the direction of travel, respectively. This suggesting that the solution may well be a strict upper bound for elliptic contact. Indeed, there have been instances in the literature where the solution for a circular contact region has been used with the assumption (incorrectly) that it also applies to an elliptic contact region. There is clearly a need for accurate solutions for a range of b/a. At the same time there is a need to independently verify that the kinematic assumptions of Ponter et al. (1985) are essentially correct for, at least, the case $b/a = 1$. This is the purpose of this paper. We also investigate the effect of a frictional load that acts at an angle to the direction of rolling.

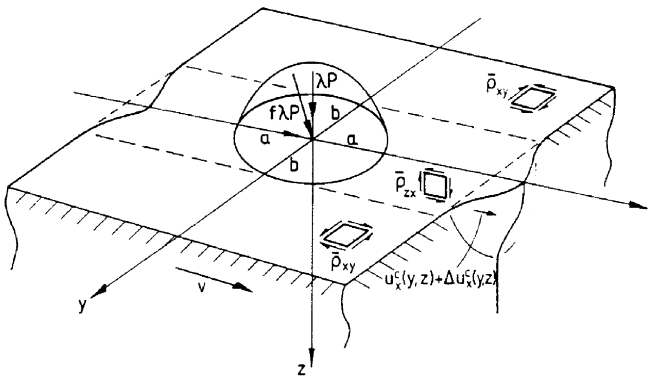

Mode of deformation in point contact: displacement of a surface segment $u_x^{\xi}(y,z)$.

Fig. 1. Rolling contact problem considered by Ponter et al. (1985).

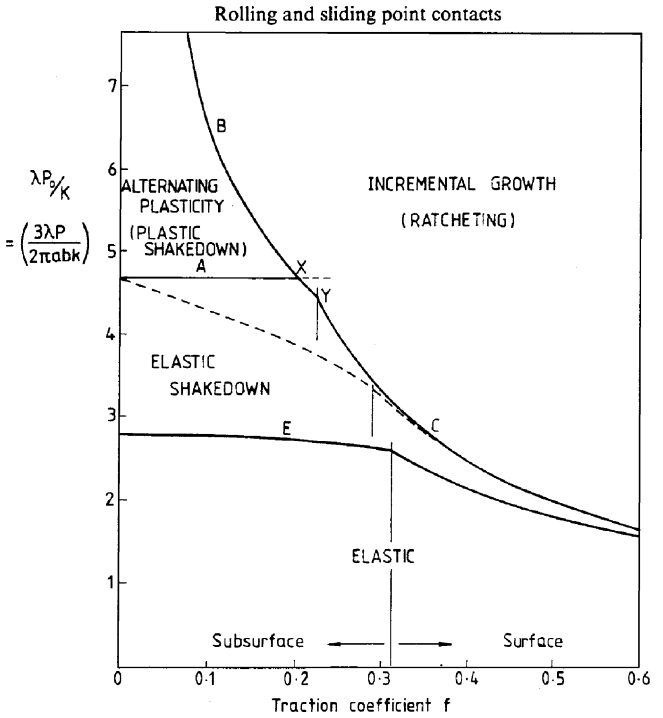

Fig. 2. Shakedown and ratchet boundary diagram for the Hertzian rolling circular contact problem ($a = b$); solution given by Ponter et al. (1985).

These objectives are achieved by a numerical method that seeks the mechanism, from within a class of mechanisms described by a finite element mesh, that minimises the upper bound shakedown limit. The method, the Linear Matching Method (Ponter and Engelhardt, 2000; Chen and Ponter, 2001; Ponter et al., 2002), is essentially a programming method that seeks mechanisms that produce a reducing sequence of upper bounds, converging to a least upper bound. For each iteration a linear problem is solved that matches the conditions of the non-linear problem in two respects. The material coefficients of the linear problem are chosen so that the linear material and the yield condition give rise to the same stress at the current estimate of the plastic strain rate history and; the load is chosen as the current least upper bound. The basic idea, as an ad hoc method, has been applied in pressure vessel design for some years and developed by Mackenzie et al. (1996), Boyle et al. (1997) and Seshadri and Mangalaramanan (1997) and is most widely known as the Elastic Compensation method.

The Linear Matching Method is here applied to the same class of rolling and sliding contact problems as discussed by Ponter et al. (1985) with the following objectives: to develop a general method capable of solving such contact problems; to observe the range of conditions when the particular type of mechanism chosen by Ponter, Hearle and Johnson is optimal; to provide shakedown limits for a range of b/a; and to explore the effect of a direction of sliding that differs from the direction of travel.

2. The upper bound shakedown theorem

The material considered is assumed to be isotropic, elastic–perfectly plastic and to satisfy the von Mises yield condition. The problem consists of a body V with boundary S, which experiences a history of

cyclic load $\lambda P_i(x_j, t)$ on S_T. λ is a load parameter. The displacement rate $\dot{u}_i = 0$ is applied on S_u. S_T and S_u are complementary parts of the boundary S. The linear elastic solution to the problem is denoted by $\lambda\hat{\sigma}_{ij}(x_i, t)$.

The upper bound shakedown theorem is expressed in terms of an incompressible and kinematically admissible strain rate history $\dot{\varepsilon}^c_{ij}$, which need not be compatible but is associated with a compatible strain increment $\Delta\varepsilon^c_{ij}$ such that

$$\int_0^{\Delta t} \dot{\varepsilon}^c_{ij}\,\mathrm{d}t = \Delta\varepsilon^c_{ij} \tag{1}$$

which in turn is associated with the corresponding displacement increment field Δu^c_i,

$$\Delta\varepsilon^c_{ij} = \frac{1}{2}\left(\frac{\partial\Delta u^c_i}{\partial x_j} + \frac{\partial\Delta u^c_j}{\partial x_i}\right) \tag{2}$$

In terms of the load history described above the upper bound shakedown limit is given by

$$\lambda_{\mathrm{UB}}\int_V\int_0^{\Delta t}(\hat{\sigma}_{ij}\dot{\varepsilon}^c_{ij})\,\mathrm{d}t\,\mathrm{d}V = \int_V\int_0^{\Delta t}\sigma^c_{ij}\dot{\varepsilon}^c_{ij}\,\mathrm{d}t\,\mathrm{d}V \tag{3}$$

where σ^c_{ij} is the stress at yield associated with $\dot{\varepsilon}^c_{ij}$ and $\hat{\sigma}_{ij}$ is the linear elastic solution associated with the load history $P(t)$. $\lambda_{\mathrm{UB}} \geqslant \lambda_s$ is an upper bound to the shakedown load parameter λ_s. For the von Mises yield condition Eq. (3) can be simplified as

$$\lambda_{\mathrm{UB}} = \frac{\int_V\int_0^{\Delta t}\sigma_y\bar{\dot{\varepsilon}}(\dot{\varepsilon}^c_{ij})\,\mathrm{d}t\,\mathrm{d}V}{\int_V\int_0^{\Delta t}(\hat{\sigma}_{ij}\dot{\varepsilon}^c_{ij})\,\mathrm{d}t\,\mathrm{d}V} \tag{4}$$

where $\bar{\dot{\varepsilon}} = \sqrt{\frac{2}{3}\dot{\varepsilon}_{ij}\dot{\varepsilon}_{ij}}$ is the effective strain rate and σ_y denotes the uniaxial yield stress. For a given load history, we seek the kinematically admissible strain rate history that minimises the upper bound (4) within a class of displacement fields described, for example, by a particular finite element mesh.

3. The Linear Matching Method

The general programming method described by Ponter and Engelhardt (2000) consists of defining a sequence of linear problems where the linear coefficients are chosen so they match the yield condition. For a von Mises yield condition the relevant linear material is incompressible with a shear modulus μ. A single step in the method begins with a kinematically admissible history of plastic strain rate $\dot{\varepsilon}^i_{ij}$, in terms of which the following linear problem is posed for a new history $\dot{\varepsilon}^f_{ij}$:

$$\dot{\varepsilon}^{f'}_{ij} = \frac{1}{\mu}(\lambda^i_{ub}\hat{\sigma}_{ij} + \bar{\rho}^f_{ij})', \quad \dot{\varepsilon}^f_{kk} = 0, \quad \text{and} \quad \mu = \frac{\sigma_y}{\bar{\dot{\varepsilon}}^i} \tag{5}$$

subject to the condition that $\dot{\varepsilon}^f_{ij}$ is also a kinematically admissible strain rate history and $\bar{\rho}^f_{ij}$ is a constant equilibrium residual stress field. The equation for μ comes from matching the linear material to the perfectly plastic material so that they both give the same effective stress corresponding to $\dot{\varepsilon}^i_{ij}$. Here $\dot{\varepsilon}^{f'}_{ij}$ refers to the deviator component of $\dot{\varepsilon}^f_{ij}$ and this notation is used throughout. Note that $\lambda = \lambda^i_{\mathrm{UB}}$, the upper bound (4) corresponding to $\dot{\varepsilon}^i_{ij}$. Integration of (5) over the cycle of loading produces the following equation relating $\Delta\varepsilon^{f'}_{ij}$ and $\bar{\rho}'^f_{ij}$:

$$\Delta\varepsilon^{f'}_{ij} = \frac{1}{\mu}(\bar{\rho}'^f_{ij} + \sigma'^{in}_{ij}) \tag{6}$$

where

$$\sigma'^{in}_{ij} = \bar{\mu}\left\{\int_0^{\Delta t} \frac{1}{\mu(t)} \lambda^i_{\mathrm{UB}} \hat{\sigma}'_{ij}(t)\,\mathrm{d}t\right\} \quad \text{and} \quad \frac{1}{\bar{\mu}} = \int_0^{\Delta t} \frac{1}{\mu(t)}\,\mathrm{d}t. \tag{7}$$

The solution to this incompressible linear problem yields a new upper bound λ^f_{UB} by substituting $\dot{\varepsilon}^f_{ij}$ into (4) which satisfies (Ponter and Engelhardt, 2000),

$$\lambda^f_{ij} \leqslant \lambda^i_{ij} \tag{8}$$

with equality if and only if $\dot{\varepsilon}^f_{ij} \equiv \dot{\varepsilon}^i_{ij}$. Hence the repeated application of this algorithm produces a monotonically reducing sequence of upper bounds that converges to a minimum upper bound. A general discussion of the method has been given by Ponter et al. (2002). If the linear problems are solved using a finite element method then the sequence converges to the least upper bound associated with the class of displacement fields defined by the finite element mesh. In this, very general, statement of the method the solution is an intrinsic property of the entire elastic stress history $\hat{\sigma}_{ij}$. There are many problems where it is possible to identify instants during the cycle when inelastic strains occur and the relationships (7) may be reduced to a finite sum with a predetermined number of terms (Ponter and Engelhardt, 2000; Chen and Ponter, 2001). For rolling and sliding contact problems this is not generally the case and the integrals (7) need to be made over the entire elastic stress history, as discussed below.

4. Application of the method to rolling and sliding contact problems

Consider a body of infinite extent in a cartesian axis direction x. The body is then defined by its geometry shape in the orthogonal (y, z) plane. A rolling and sliding contacting body passes, quasi-statically, along a line of travel in the x direction. As a typical material element in each (y, z) cross-section of the body experiences an identical history of elastic stress, any resultant deformation field will vary within a (y, z) plane but will be independent of x. Hence $\dot{\varepsilon}^c_{ij}$, $\Delta\varepsilon^c_{ij}$ and Δu^c_i are all independent of x and depend only on y and z. The history of the linear elastic solution at a fixed material point x_i may be written in the general form:

$$\hat{\sigma}_{ij}(x_i, t) = \hat{\sigma}_{ij}(x + vt, y, z) \tag{9}$$

where v is the velocity of travel of the contacting body. A single cycle of loading for a material element in the plane $x = 0$ consists of $-t_0 \leqslant t \leqslant t_0$ where t_0 is sufficient large for the elastic stress at $(\pm vt_0, y, z)$ to be negligibly small. In the following we apply these characteristics of the problem directly to the finite element solution method.

Although the upper bound (4) is expressed in terms of the entire history of the elastic stress, at each point in the (y, z) plane the contribution to the total accumulated strain $\Delta\varepsilon^c_{ij}$ usually occurs at one or two instants during the cycle when the extremes of the elastic stress history occur. We discretise the problem by dividing up the cycle of loading into $r - 1$ equal time intervals and hence r instants when plastic strains may potentially occur. The integral (1) becomes the finite sum:

$$\Delta\varepsilon^c_{ij} = \sum_{n=1}^{r} \Delta\varepsilon^n_{ij} \tag{10}$$

Hence the linear problem for a new kinematically admissible strain rate $\Delta\dot{\varepsilon}^f_{ij}$ and a time constant residual stress field $\bar{\rho}^f_{ij}$ may be defined by (5) where

$$\sigma'^{in}_{ij} = \bar{\mu}\left\{\sum_{n=1}^{r} \frac{1}{\mu_n} \lambda \hat{\sigma}'_{ij}(t_n)\right\} \tag{11a}$$

and

$$\frac{1}{\bar{\mu}} = \sum_{n=1}^{r} \frac{1}{\mu_n} \quad \text{where } \mu_n = \frac{\sigma_y}{\bar{\varepsilon}(\Delta\varepsilon_{ij}^{ni})} \tag{11b}$$

Convergence of the method with respect to r then consists of increasing the number of time intervals until there is a negligible change in the solution.

5. Implementation of the method

A very significant advantage of the method comes from the ability to use standard commercial finite element codes that have the facility to allow the user to define the material behaviour. This has been done in the code ABAQUS (2001) of HKS Ltd. using a method devised by Engelhardt (1999). Essentially, ABAQUS carries out a conventional step-by-step analysis and, through the implementation of user routines, each increment is reinterpreted in terms of an iteration of the method.

By this means it is possible to implement the method exactly, except for a numerical approximation. The integration involved in the evaluation of the stiffness matrix for each linear problem uses Gaussian integration which would be exact if the linear coefficients were constant within the element. As the linear coefficients vary spatially this condition is not satisfied. From experience from comparisons with exact solutions, this numerical error is not regarded as significant. The choice and density of the finite element mesh defines the accuracy of the solution.

6. The finite element model and loading condition for rolling and sliding contacts

The above numerical procedure has been used to solve the rolling and sliding contact problem discussed by Ponter et al. (1985). We consider an elastic–perfectly plastic half space over whose surface a prescribed traction is repeatedly traversed. In all cases the normal surface pressure $p(x, y)$ is given by the Hertzian distribution of pressure,

$$p(x,y) = p_0[1 - (x/a)^2 - (y/b)^2]^{1/2} \tag{17a}$$

acting on the elliptical area of semi-axes a and b where, here, $x = y = 0$ corresponds to the centre of contact area. When sliding accompanies rolling an additional shear traction occurs,

$$q(x,y) = fp_0[1 - (x/a)^2 - (y/b)^2]^{1/2} \tag{17b}$$

where f is the coefficient of friction and will be taken to act in the direction of travel when $a \neq b$. An analytic linear elastic solution for the general elliptic case has been given by Sackfield and Hills (1983) and Hamilton (1983) for a circular contact region.

First we consider a circular contact problem where the frictional contact stresses may act at an angle to the direction of travel. Such a circumstance may occur when, for example, a spherical ball simultaneously rolls and slides on a surface with the axis of rotation at an angle to the direction perpendicular to the direction of travel. The resulting direction of slide of the contacting region is the resultant of sliding due to the travel of the centre of the ball and sliding due to the rotation of the ball. Hence the direction of travel and the direction of slide may not coincide. Accepting the simplifications introduced by Hertz and Mindlin, the boundary stresses are given within a circle of radius a by Hamilton (1983):

$$\sigma_z = \frac{3P}{2\pi a^3}(a^2 - x^2 - y^2)^{1/2} \tag{18a}$$

$$\tau_{zx} = \frac{3F}{2\pi a^3}(a^2 - x^2 - y^2)^{1/2} \tag{18b}$$

$$\tau_{zy} = \frac{3Q}{2\pi a^3}(a^2 - x^2 - y^2)^{1/2} \tag{18c}$$

where $x^2 + y^2 \leqslant a^2$. Here $P = 2/3(p_0\pi a^2)$ is the total normal force in the z direction, F is the total tangential force in the y direction, perpendicular to the direction of travel, and Q is the total frictional force in the direction of travel, the x direction as shown in Fig. 3. All the boundary stresses outside the circle of contact are zero. The coefficient of friction f and the angle θ between the x direction and the resultant frictional force (i.e. the resultant direction of slide) are given by

$$f = \frac{\sqrt{F^2 + Q^2}}{P}, \quad \tan\theta = \frac{F}{Q} \tag{19}$$

The radius of the circle of contact a is given by the well-known Hertzian expression:

$$a = \left\{\frac{3\pi PR}{4}\left[\frac{1 - v^2}{\pi E}\right]\right\}^{1/3} \tag{20}$$

where E and v are Young's modulus and Poisson's ratio of the half plane and R is the radius of curvature of the contacting sphere, assumed rigid. The analytical elastic stress field in the half space for circular contact under the combined action of P, Q and F is obtained by supposition of the solution for the frictional force in the direction of travel (given by Hamilton, 1983) and the same solution rotated by 90° about the z axis.

In this solution we assume that the boundary stresses are given by the Hertzian solutions. This presupposed that any grooving of the surface due to transient strains before shakedown will have no effect on the Hertzian solution. This, of course, also applies to the assumptions made by Ponter et al. (1985).

Considering the property of the half space, we take a cuboid with the size of $40a \times 20a \times 2a$, discretised by 3-D 8-node isoparametric finite elements. All cross-sections of the half space in the (y, z) plane experience the same distribution of displacement, which is therefore independent of x. In principle a solution could be obtained by using a mesh with only a single element in the x direction, but we find the best solutions are obtained by allowing a significant number of elements in the x direction. We then impose the boundary condition on the two faces $x =$ constant that the nodal displacements at nodes with the same (y, z) co-ordinates have the same displacements. Such linked node boundary conditions are a standard feature of ABAQUS. Zero-displacement constraints are imposed on the remaining three surfaces except the top surface $z = 0$. The detailed mesh arrangements on three faces of the model are shown in Figs. 4–6.

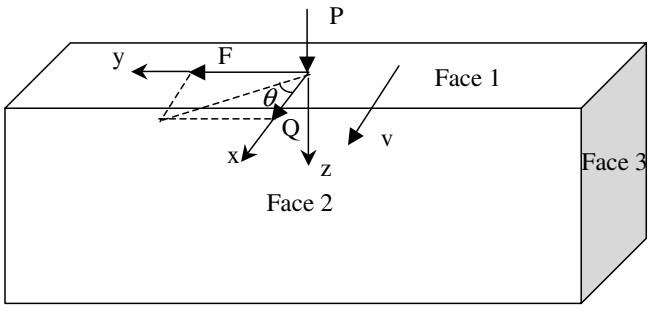

Fig. 3. The model for point contact; the x axis is the direction of rolling.

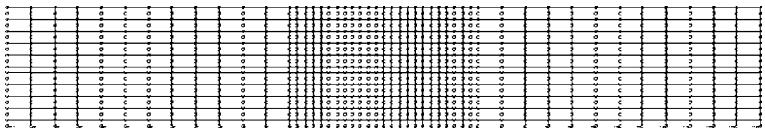

Fig. 4. The mesh arrangement in face 1 of model 3 (48×20 elements).

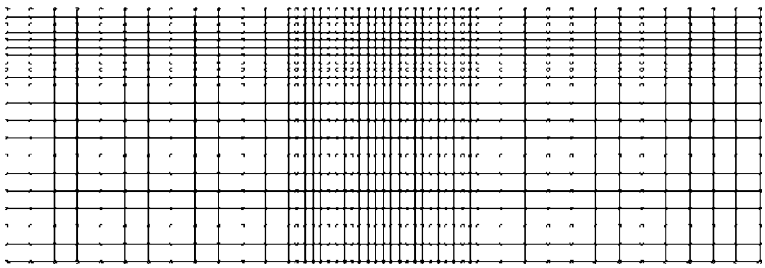

Fig. 5. The mesh arrangement in face 2 of model 3 (48×20 elements).

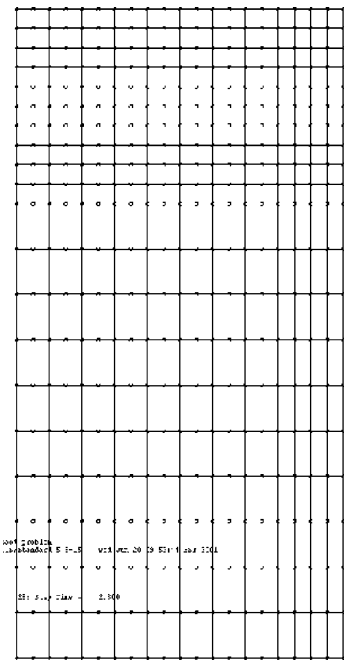

Fig. 6. The mesh arrangement in face 3 of model 3 (20×20).

The total number of elements is up to 19,200. It can be seen in these figures that in order to optimise the numerical efficiency and accuracy, the finite element mesh has been chosen to make the distribution of the elements near the contact area more dense than those distributed in other parts of the structure. A detailed discussion of the effects on the results of the mesh geometry and the number of time instants r will be presented later.

7. Numerical results for rolling and sliding point contacts

Converged solutions for a circular contact region are presented in Fig. 7 in the form of an interaction diagram where $k = \sqrt{3}\sigma_y$ denotes the shear yield stress. Solutions for $\theta = 0$ may be directly compared with the solution of Ponter et al. (1985) reproduced here as Fig. 2. For $f \leqslant 0.15$ the shakedown limit is a reverse plasticity limit where the plastic strain history consists of equal and opposite plastic strains occurring at two distinct instants, resulting in zero accumulation of plastic strain over the cycle (Figs. 8–10). The numerical solution reproduces the solution of Fig. 2 very accurately. In Fig. 11 the optimal mechanism is shown for $f = 0.1$ as a contour plot of constant $\bar{\varepsilon}(\Delta\varepsilon_{ij}^k)$. The strain is concentrated at a single point corresponding to the maximum variation in effective stress in the elastic solution where the reverse plasticity mechanism occurs. For $f \geqslant 0.15$ the numerical solutions indicate that a global ratcheting mechanism is activated, similar in form to that assumed by Ponter et al. For $f = 0.2$ the numerical solution is slightly below the Ponter solution but lies slightly above for $f = 0.6$. The optimal mechanism for $f = 0.25$ is shown in Fig. 12. The type of mechanism assumed by Ponter et al. where deformation is confined to a slip band surrounding the loaded surface is clearly reproduced although there is a distinct gradient of strain, produced partially by the nature of the finite element displacement fields and partially by the averaging process involved in the standard ABAQUS plotting routines. Fig. 13 shows strain contours for $f = 0.6$ showing the strain concentrated at the surface, again in accordance with Ponter et al. The general nature of the Ponter, Hearle and Johnson solutions is clearly correct although the assumption that deformation occurs only in the direction of travel is clearly an approximation for intermediate values of f. However, the displacement fields generated by the finite element approximation cannot easily reproduce the slip surfaces assumed in the Ponter solution that are clearly optimal for higher values of f when the ratcheting mechanism coincides with the surface. Figs. 14–16 show plots for $Q = 0$, i.e. the frictional force acting in a direction perpendicular to the direction of rolling acting to the left. The nature of the mechanism is similar to the $F = 0$ case, except that the distribution is biased towards the direction of the frictional force involving

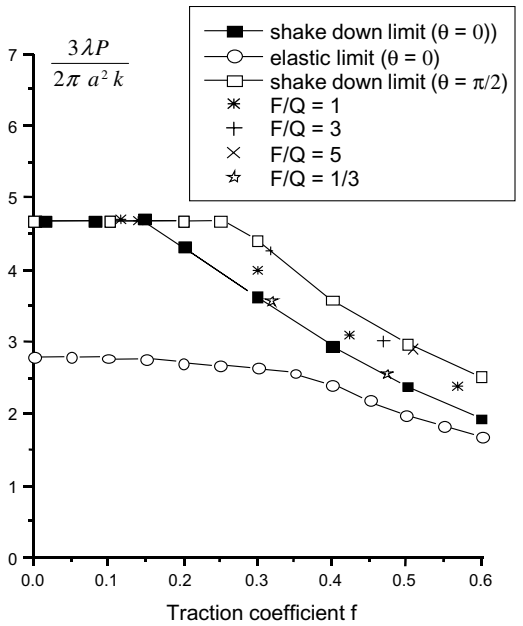

Fig. 7. Shakedown and elastic limit of a circular loaded region for different normal and tangential loads.

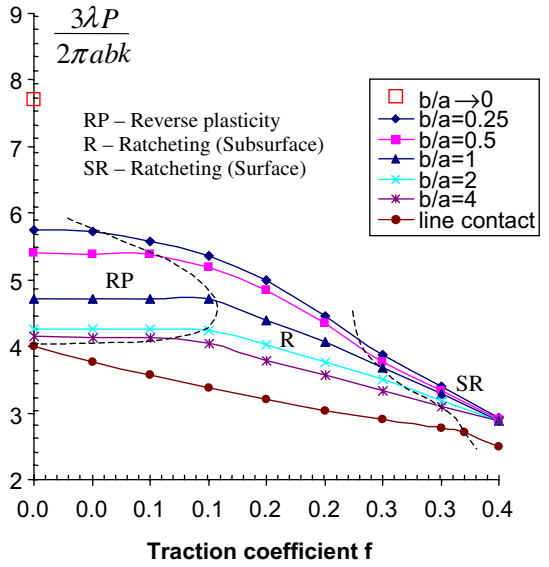

Fig. 8. Shakedown limit of an elliptical loaded region for different normal and tangential loads ($\theta = 0$).

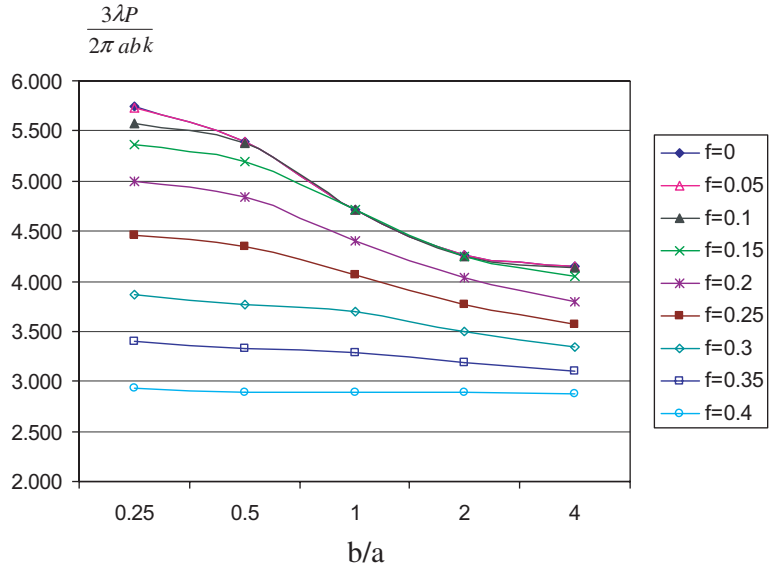

Fig. 9. Variation of shakedown limits with shape of loaded ellipse (b/a) for different normal and tangential loads ($\theta = 0$).

deformation in that direction. Figs. 17–19 shown strain plots for intermediate cases showing, again, similar behaviour.

For the case of an elliptic contact area, elastic solutions given by Sackfield and Hills (1983) only include the case where the frictional force acts in the direction of travel. A complete set of optimal solutions for $0 \leqslant f \leqslant 0.4$ and $0.25 \leqslant b/a \leqslant 4$ are shown in Fig. 8 where the load is divide by the area of the ellipse. The solutions are also shown in Fig. 9 in the form of contours of constant f.

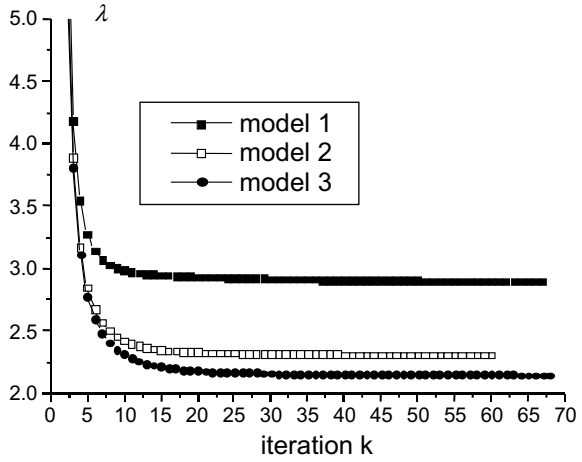

Fig. 10. The convergence conditions for the three finite element models listed in Table 1.

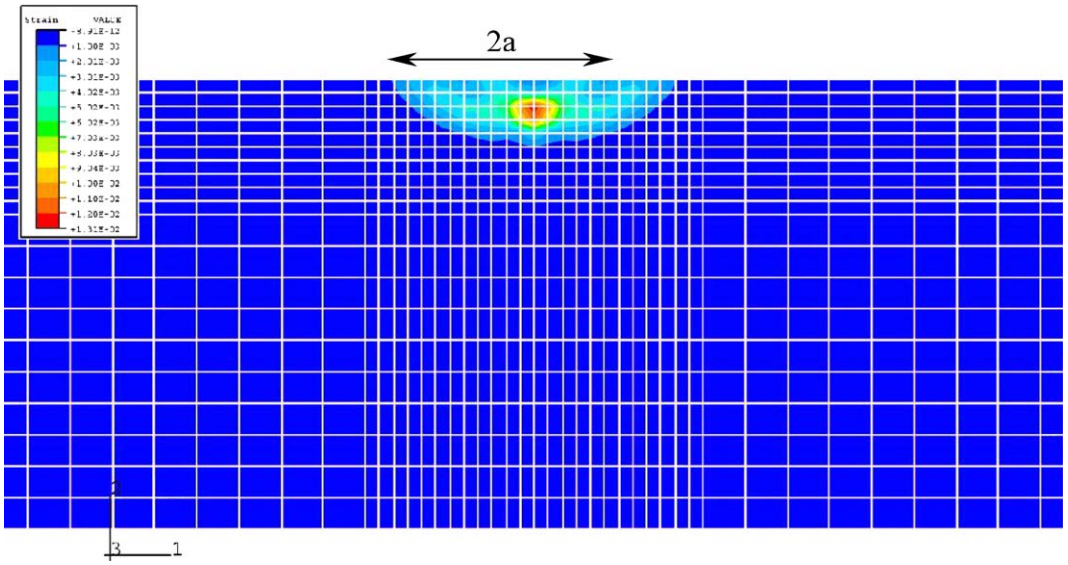

Fig. 11. Contours of constant von Mises effective strain for the convergent mechanism; frictional force in direction of travel, $F = 0$, $a = b$, $f = 0.1$.

For large b/a the solutions would be expected to converge towards the line contact solution. The analytic solution, based upon the line contact elastic solution (Johnson, 1985), is shown for comparison and lies below but close to the solutions for $b/a = 4$. There are, however, distinct differences. For line contact and $f = 0$, a reverse plasticity mechanism and ratcheting below the surface yield identical shakedown loads. For $f \geqslant 0$, the subsurface ratcheting mechanism yields a lower shakedown load. For $f \geqslant 0.34$, the ratchet mechanism lies at the surface. For $b/a = 4$, a reverse plasticity solution dominates for a significant range of f before a subsurface mechanism dominates. By inspection of the strain plots for the optimal mechanisms it is possible to identify regions of the interaction diagram where the three principal mechanism types operate,

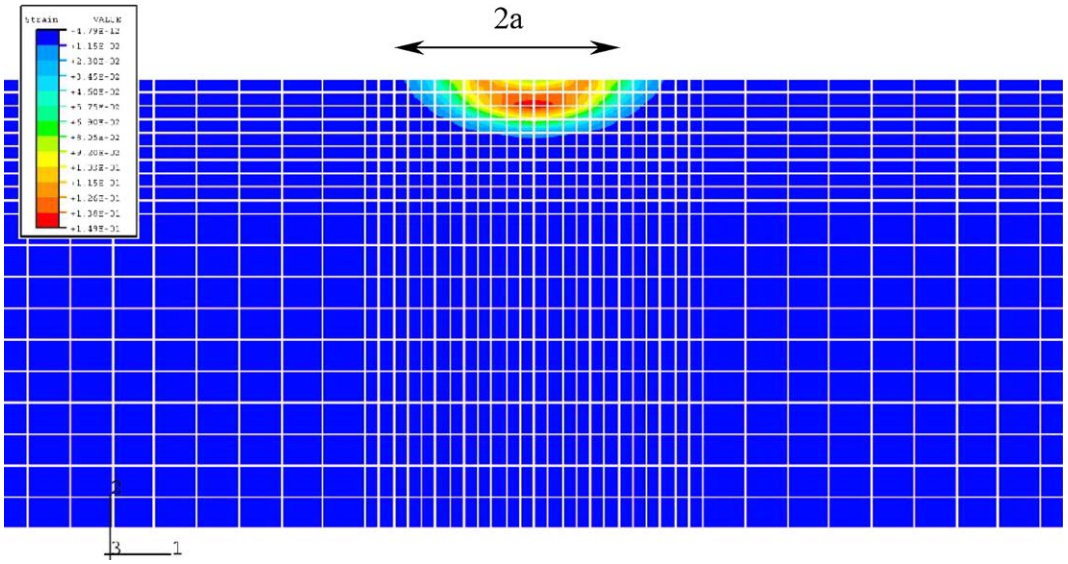

Fig. 12. Contours of constant von Mises effective strain for the convergent mechanism; frictional force in direction of travel, $F = 0$, $a = b$, $f = 0.25$.

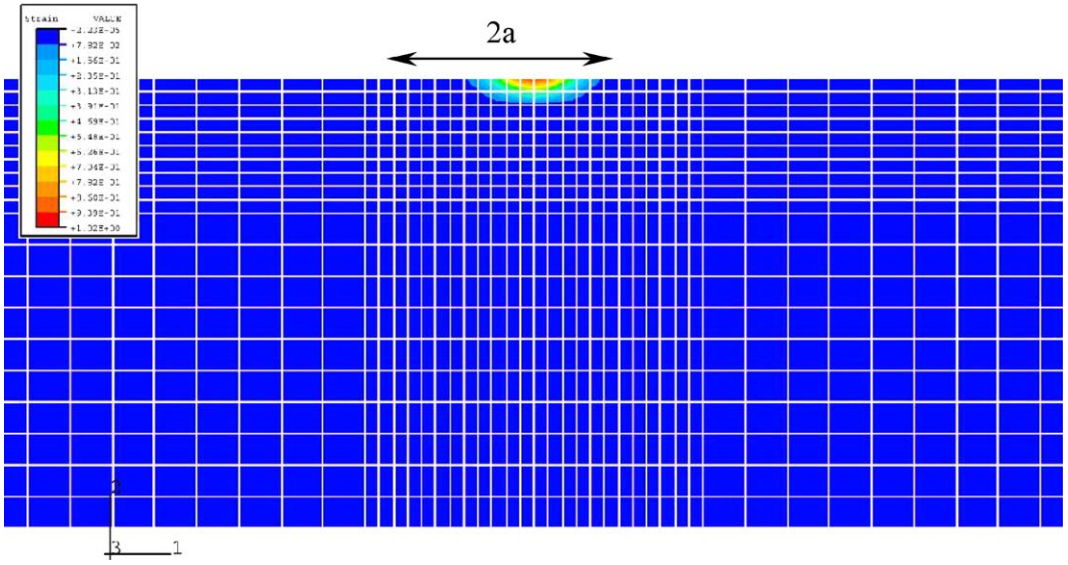

Fig. 13. Contours of constant von Mises effective strain for the convergent mechanism; frictional force in direction of travel, $F = 0$, $a = b$, $f = 0.6$.

labeled as RP for reverse plasticity, R for subsurface ratchet mechanism and SR for surface ratchet mechanism. The boundaries between these regions are shown in Fig. 8; these boundaries are necessarily approximate. For large b/a, the solution for $f = 0$ may be expected to converge to either the limit load solution or the reverse plasticity solution for the indentation problem. The lesser of these, the limit load solution, as-

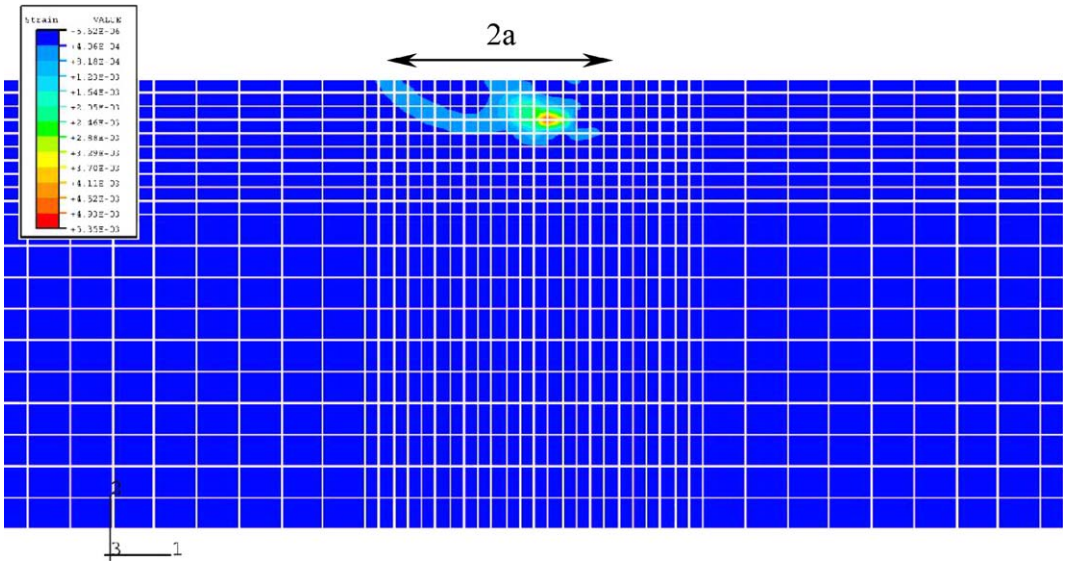

Fig. 14. Contours of constant von Mises effective strain for the convergent mechanism; frictional force perpendicular to the direction of travel, $Q = 0$, $a = b$, $f = 0.1$.

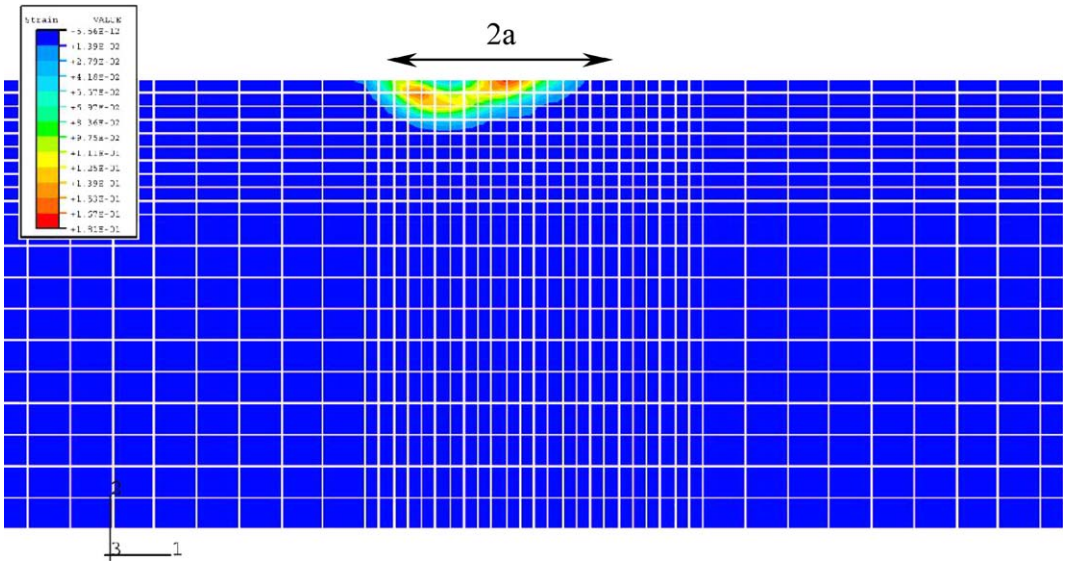

Fig. 15. Contours of constant von Mises effective strain for the convergent mechanism; frictional force perpendicular to the direction of travel, $Q = 0$, $a = b$, $f = 0.25$.

sumed to be the Prandtl solution, is shown as the case $b/a \to 0$. This solution is significantly greater than the solution for $b/a = 0.25$.

For all values of b/a, the shakedown limits are near identical for $f = 0.4$ where the mechanism is localised ratcheting on the surface.

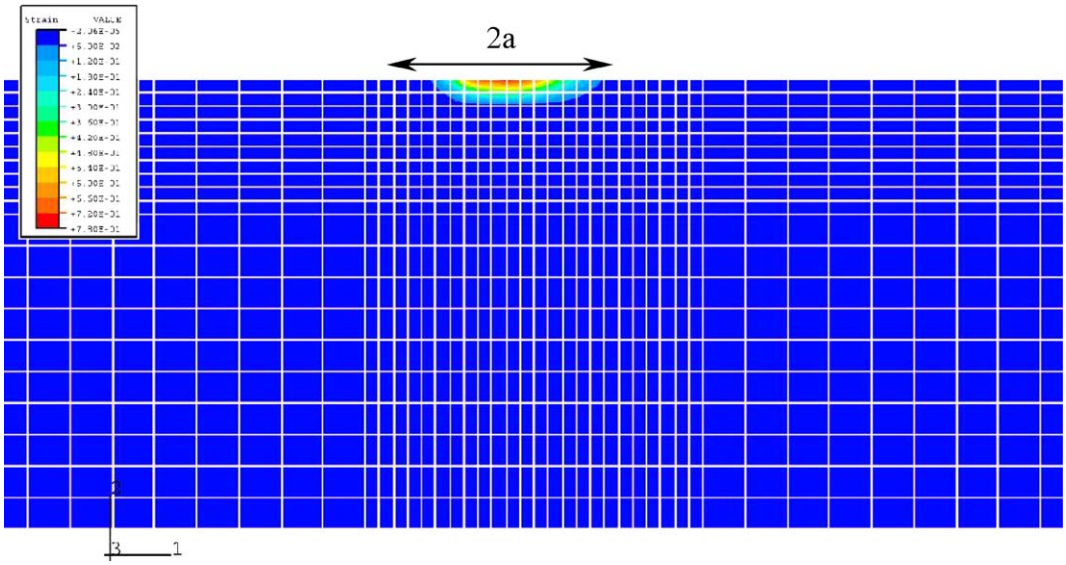

Fig. 16. Contours of constant von Mises effective strain for the convergent mechanism; frictional force perpendicular to the direction of travel, $Q = 0$, $a = b$, $f = 0.6$.

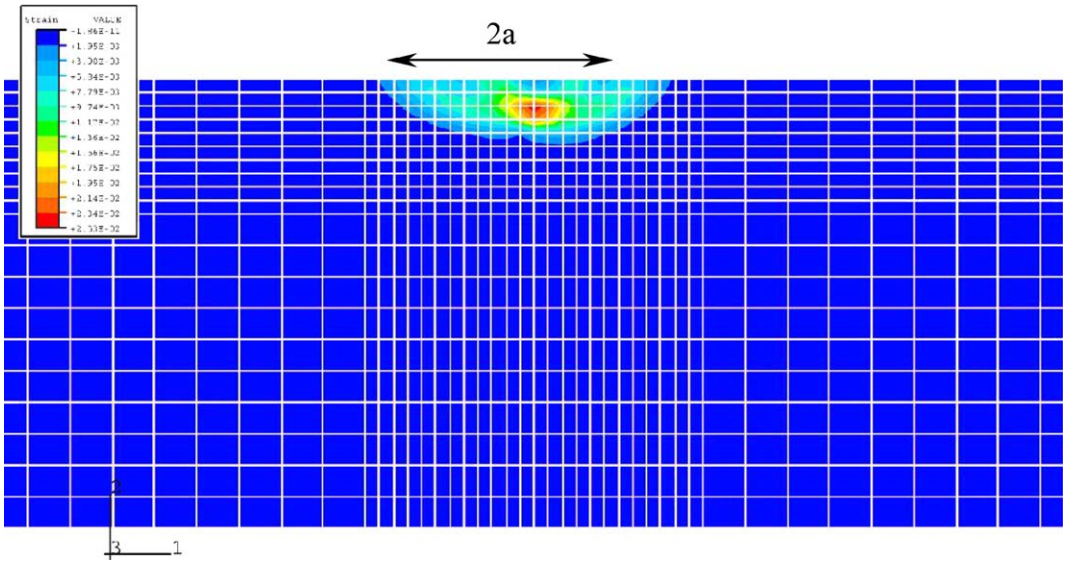

Fig. 17. Contours of constant von Mises effective strain for the convergent mechanism; frictional force at $\theta = 45°$ to the direction of travel, $a = b$, $f = 0.1$.

8. Numerical issues—factors that affect the accuracies of solutions

8.1. The effects of mesh arrangement

The solutions discussed above were obtained for a finite element mesh and set of loading instants chosen as result of a process of optimisation, described below. The displacement field in the upper bound is inde-

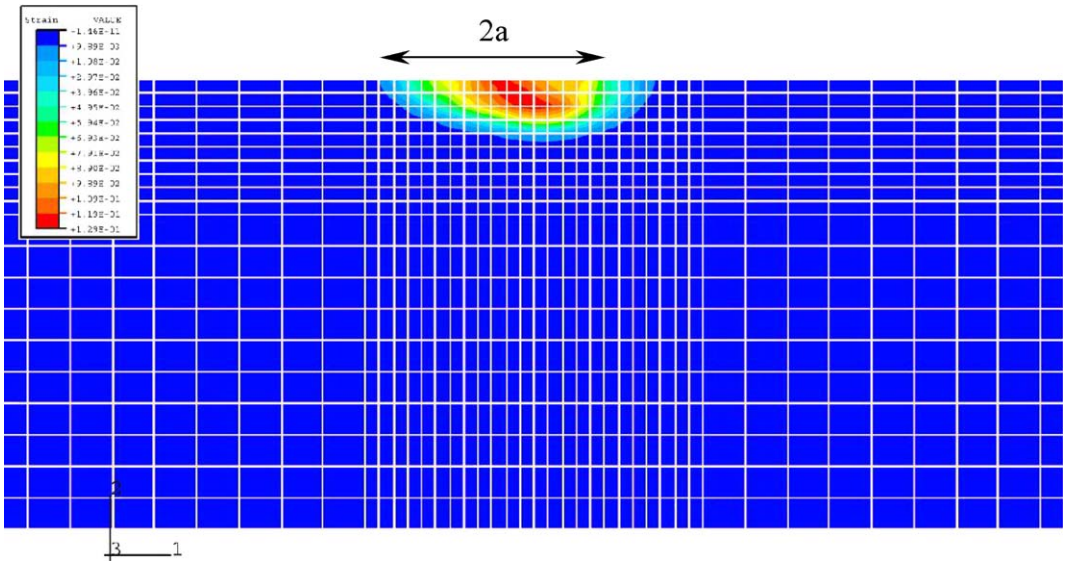

Fig. 18. Contours of constant von Mises effective strain for the convergent mechanism; frictional force at $\theta = 45°$ to the direction of travel, $a = b$, $f = 0.18$.

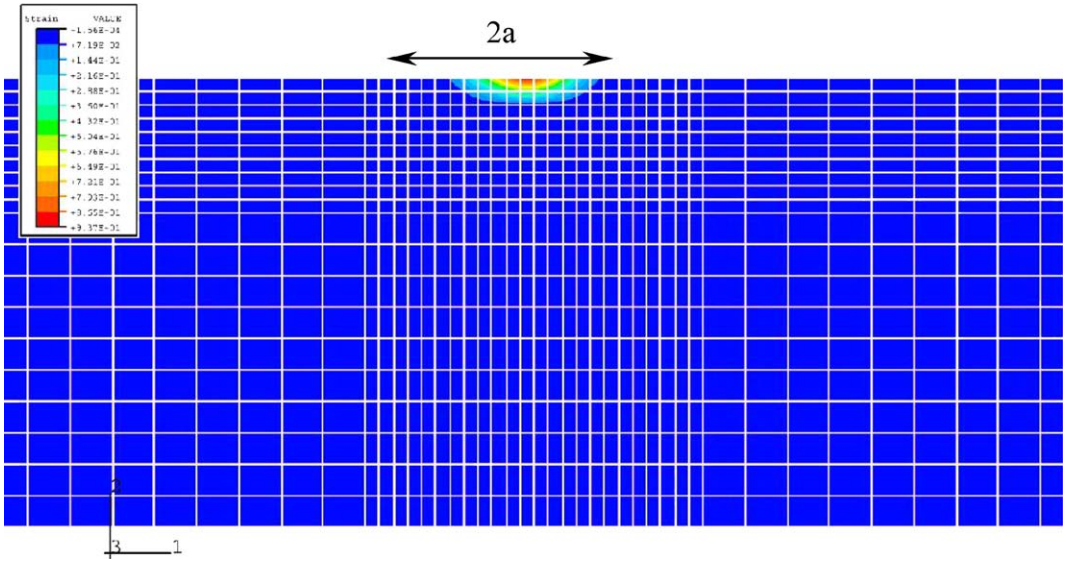

Fig. 19. Contours of constant von Mises effective strain for the convergent mechanism; frictional force at $\theta = 45°$ to the direction of travel, $a = b$, $f = 0.4$.

pendent of the axis x in the direction of travel. In principle only a single layer of elements is required in the x direction. However, as a result of numerical trials we find that lower upper bounds may be found by including a number of elements in the x direction, and the final choice arose from comparisons of the converged solutions for $f = 0$ for a number of mesh arrangements. The convergence of the upper bound with iterations for three typical finite element models with differing mesh arrangement is shown in Fig. 10 with

Table 1
The mesh arrangement in the different finite element models discussed in Fig. 10 ($Q = 0.15P$, $F = 0.45P$, $f = 0.474$)

Model	No. of element along y direction	No. of element along x direction	No. of element along z direction	No. of element in the model
Model 1	36	10	30	10,800
Model 2	40	20	20	16,000
Model 3	48	20	20	19,600

Table 2
The effects of the number of load instants on the shakedown limit

No. of load instants	Converged upper bound λ	Iterations to convergence	Total CPU time (s)
4	3.6863	45	18,858
12	3.3771	50	21,017
22	3.3327	64	26,832
42	3.3267	71	30,158

details in Table 1. For all three models, the total numbers of the elements exceeds 10,000. However, the final converged shakedown limit multipliers λ differ significantly. Model 1, which yields the poorest result, differs from Models 2 and 3 by having only half the element number in the x direction, indicating the need for a significant number of elements in the direction of travel. The chosen Model 3, for the solutions described above, also involves a greater number of elements in the transverse y direction. The rate of convergence in all three cases is similar and a converged solution for λ was obtained in 30–70 iterations assuming no change in the 7th significant figure for two consecutive iterations.

8.2. The effects of the number of load instance

Table 2 shows the variations of the shakedown multiplier, iteration number and total CPU time with the number of load instants r. The optimal upper bound reduces with r and reaches a stable value when r approaches 40. The value of $r = 42$ was used in the solutions described above as higher values increased the CPU time without significant change in the solution. It is evident from these studies that careful optimisation of the mesh geometry and the number of load instants have a significant effect on converged solutions.

9. Relevance of the solutions to practical situations

The solutions described above are intended as reference solutions that supplement the widely used solution of Ponter et al. (1985). The solutions are based upon the analytic elastic solutions under Herztian contact conditions and are only strictly valid if the traction distribution remain elliptical in shape. Of course the same objection applies to the solutions of Ponter et al. (1985) which not only assumes circular contact, but also a special mechanism and hence is approximate. Hence, this paper does remove two important assumptions of Ponter et al. (1985), which, in the lack of other data in the literature, were indeed used as reference even for the non-elliptical contact cases (with clearly a large approximation)! The paper certainly improves Ponter et al. (1985) by a significant amount, but this of course does not imply that further assumptions may still be removed in future studies, probably with a significant amount of additional effort. Also, notice that the elliptical contact area assumption does not require necessarily that the *elastic* elliptical solution is used. The reference solution can also be used in "intelligent" ways if significant geometrical changes are predicted

in the contact induced by permanent deformation, by using the "effective" contact area, estimated either experimentally or with some other mean, as a starting point.

The effect of plastic strains upon the distribution of contact stresses may be understood as due to two separate components: the transient accumulation of plastic strains $\varepsilon_{ij}^{\mathrm{T}}$ that occurs during the initial passages prior to the shakedown state being achieved; and the cyclic accumulation of plastic strain per passage at and just above the shakedown limit $\Delta\varepsilon_{ij}^{p}$.

The transient strain $\varepsilon_{ij}^{\mathrm{T}}$ depends on any initial residual stress in the half space and any prior loading and is not uniquely defined. In the absence of initial residual stresses, the value of $\varepsilon_{ij}^{\mathrm{T}}$ will be dominated by the plastic strains that are required to develop the constant residual stress $\bar{\rho}_{ij}$ at the shakedown state and will remain of the order of magnitude of the elastic strains within yield. Maximum values would occur in the locations where the ratchet mechanisms occur. Of the three classes of mechanisms, the plastic strains in both the reverse plasticity mechanism and the subsurface ratchet mechanism are concentrated in regions remote from the loaded surface and hence any surface distortion will be governed in size by elastic strains. Hence the effect upon the contact stresses will depend upon the relative magnitude of the elastic moduli of the contacting body and the half space with decreasing effect as the elastic modulus of the contacting body decreases.

At the shakedown limit the increment of plastic strain per passage is zero and then increases as the load is taken above the shakedown limit. There remains the possibility that the accumulation of surface displacement may then change the shakedown limit so that either there is a reversion to a shakedown state or the ratchet rate increases. Again, the nature of the mechanisms provides insight. For loads at the reverse plasticity limit, no surface accumulation of displacement occurs. For intermediate values of the friction coefficient f, an entire region beneath the contacted area moves as a rigid body and there is no further effect upon the contact stresses. For high friction, ratcheting occurs at the surface and there is the possibility of surface rutting during which the contact conditions could change.

In summary, the solutions presented here are intended as reference solutions, of use when insight is already available into the nature of the contact area. They demonstrate, within the parameters of the solutions, the sensitivity of the shakedown state to the details of surface loading.

10. Conclusions

The paper describes a powerful and efficient numerical method for the evaluation of shakedown limits for rolling and sliding point contact problem based upon the Linear Matching Method, interpreted as a non-linear programming method for which strict convergence proofs exist, and uses this method to provide reference solutions for the general elliptical contact area Hertzian contact problem.

The analytic linear elastic solutions for elliptical and circular Hertzian contact problems provided by Sackfield and Hills (1983) and Hamilton (1983) form the basis of a series of calculations of least upper bound shakedown limits for the rolling contact of a half space for both a circular and an elliptic contact region. For accurate solutions, we show that it is necessary to optimise the finite element mesh and the number of time instants during the loading sequence.

For a circular contact area and a frictional force in the direction of travel, direct comparison was made with the semi-analytic solutions of Ponter et al. (1985). The numerical solutions generally agree with these solutions. However, it is clear that the kinematic assumption of the Ponter, Hearle and Johnson solutions, that deformation only takes place in the direction of travel, is not always strictly correct but provides a very good first approximation for $a = b$ when the frictional force is in the direction of travel. The numerical solutions produced optimal mechanisms associated with the shakedown limit that were very similar in form to those assumed by Ponter et al. New solutions are presented where the direction of the frictional loading forms an angle to the direction of travel. In all such cases the shakedown limit was increased when norma-

lised with respect to the friction coefficient, the greatest increase occurring when the frictional force acts perpendicular to the direction of travel.

Solutions are then presented for the case of an elliptic contact area and, again, with the frictional force in the direction of travel. These solutions show that the general character of the ratchet mechanisms is the same as the circular contact case. It is possible to describe the range of frictional coefficient f and ratio of principal axis b/a for which reverse plasticity, subsurface ratchet mechanisms and surface ratchet mechanisms occur. When normalised with respect the average normal pressure over the contact area, the shakedown limit monotonically decreases with b/a. For the largest value of $b/a = 4$ the limit is very close to the line contact solution, the limit as $b/a \to \infty$ and this solution forms a lower bound for all solutions. In contrast the Ponter, Hearle and Johnson (1985) solution is appreciably greater than the line contact solution for $b/a = 10$ and appears to converge to a strict upper bound with increasing b/a. The variation with b/a in our numerical solutions decreases with increasing f. For $f = 0.4$, the shakedown limit is very insensitive to b/a and the ratchet mechanism becomes very localised at the surface.

The solutions presented in this paper demonstrate that it is possible to generate accurate shakedown solutions numerically for rolling contact problems. Such solutions, when drawn together into interaction diagrams, provide broad insight into the factors that influence the onset of plastic strain growth and, therefore, are of use in design.

The solutions assume that any transient strains that occur prior to reaching a shakedown state have no effect of the Hertzian contact pressure distribution and it is not possible to exclude the possibility that such an effect occurs. However, it is not possible, at the present time, to evaluate the significance of such an effect.

Acknowledgements

HC and ARSP gratefully acknowledge the support of the Engineering and Physical Sciences Research Council of the United Kingdom during the course of this work. MC is pleased to acknowledge the support of the Ministry of Italian Research (MIUR) for funding of CEMEC – Centro di Eccellenza in Meccanica Computazionale, and for PRIN2004 prot. 2004091344_002 ''Computation of residual stresses and multiaxial fatigue criteria parameters in rolling contact fatigue''. Thanks are due to the Politecnico di Bari for support for GS during a student project period at Leicester University. Thanks are due to Alex Savoury of the Department of Engineering, Leicester University, for the analytic solution for line contact shown in Fig. 8.

References

ABAQUS, 2001. User's Manual, Version 6.2. HKS Ltd., Providence, RI, USA.

Boyle, J.T., Hamilton, R., Shi, J., Mackenzie, D., 1997. J. Pressure Vessel Technol. 119, 236–242.

Chen, H.F., Ponter, A.R.S., 2001. Int. J. Pressure Vessels Piping 78 (6), 443–451.

Engelhardt, M., 1999. PhD thesis, University of Leicester.

Ekberg, A., Kabo, E., Andersson, H., 2002. Fatigue Fract. Eng. Mater. 10, 899–909.

Hamilton, G.M., 1983. Proc. Instn. Mech. Engrs. 197C, 53–59.

Johnson, K.L., 1985. Contact Mechanics. Cambridge University Press, Cambridge.

Mackenzie, D., Boyle, J.T., Hamilton, R., Shi, J., 1996. Proceedings of the 1996 ASME PVP Conference, vol. 338, pp. 203–208.

Ponter, A.R.S., Engelhardt, M., 2000. Eur. J. Mech. A/Solids 19, 423–445.

Ponter, A.R.S., Chen, H., Boulbibane, M., Habibullah, M., 2002. In: Mang, H.A., Rammerstorfer, F.G., Eberhardsteiner, J. (Eds.), Proceedings of the Fifth World Congress on Computational Mechanics (WCCM V), Vienna, Austria. Vienna University of Technology, Austria, ISBN 3-9501554-0-6, 21 pp. Available for downloading until 2008: http://wccm.tuwien.ac.at .

Ponter, A.R.S., Hearle, A.D., Johnson, K.L., 1985. J. Mech. Phys. Solids 33 (4), 339–362.

Ringsberg, J.W., 2001. Int. J. Fatigue 23, 575–586.
Ringsberg, J.W., Josefson, B.L., 2001. Proc. Inst. Mech. Eng. Part F: J. Rail Rapid Transit 215, 243–259.
Sackfield, A., Hills, D.A., 1983. J. Strain Anal. 18, 101–105.
Seshadri, R., Mangalaramanan, S.P., 1997. Int. J. Pressure Vessels Piping 71, 93–106.